INDIAN JOURNAL OF SCIENCE AND TECHNOLOGY

ORIGINAL ARTICLE

Global Stability and Sensitivity Analysis of n-Compartment SEI($Q_1Q_2...Q_{n-4}$)R Model with Single Dose Vaccination

Sarita Jha[1], Prabhat Kumar Mandal[2], Govind Kumar Jha[2]*

1 Department of Mathematics, K.B.Women's College, Hazaribagh-825301, Jharkhand, India
2 University Department of Mathematics, Vinoba Bhave University, Hazaribagh-825301, Jharkhand, India

OPEN ACCESS

Received: 15/09/2025
Accepted: 06/11/2025
Published: 31/12/2025

Citation: Jha S, Mandal PK, Jha GK (2025) Global Stability and Sensitivity Analysis of n-Compartment SEI($Q_1Q_2...Q_{n-4}$)R Model with Single Dose Vaccination. Indian Journal of Science and Technology 18(48): 3993-4005. https://doi.org/10.17485/IJST/v18i48.1585

* **Corresponding author**.

jhagovi@gmail.com

Funding: None

Competing Interests: None

Published By Indian Society for Education and Environment (iSee)

ISSN
Print: 0974-6846
Electronic: 0974-5645

Abstract

Objectives: This work develops and analyzes an extended SEI($Q_1Q_2...Q_{n-4}$)R framework that incorporates several quarantine zones, vaccination, and partial immunity to better understand epidemic behavior. **Methods**: The proposed framework is formulated as a nonlinear system of ordinary differential equations. The basic reproduction number is derived using the next-generation matrix method, while Lyapunov functions and LaSalle's invariance principle are applied to establish global stability of the disease-free and endemic equilibria. Sensitivity analysis quantifies the influence of transmission, vaccination, and recovery parameters, and MATLAB (R2024a)-based simulations employing literature-supported parameter values are used for validation. **Findings:** The analysis establishes that the disease-free equilibrium is globally asymptotically stable when the basic reproduction number is below unity, whereas an endemic equilibrium persists when it exceeds one. Sensitivity and simulation analyses collectively validate these theoretical outcomes, identifying vaccination rate, vaccine efficacy, transmission rate, and recovery parameters as the most influential factors. Simulations of the generalized n-compartment model for n=5 and n=7 confirm that the compartmental dynamics follow the analytical stability patterns; moreover, increasing quarantine compartments effectively lowers infection peaks and accelerates recovery. **Novelty**: This study introduces a unified integer-order epidemic framework that generalizes to any number of compartments, allowing flexible modeling of outbreaks with multiple quarantine zones and vaccination effects. Its analytical formulation, independent of compartment count, offers a scalable foundation for evidence-based epidemic control and public health decision-making.

Keywords: Epidemiology; Equilibria; Global Stability; Sensitivity Analysis; n compartmental model

1 Introduction

Mathematical modeling plays a vital role in understanding and predicting the transmission patterns of infectious diseases. Such models serve as essential tools for evaluating intervention strategies, including quarantine, vaccination, and social distancing measures. Classical compartmental frameworks such as SIR, SEIR, and their modern extensions have remained the backbone of epidemic modeling and are extensively applied to study the spread of diseases like COVID-19, influenza, and SARS-CoV-2[1],[2],[3]. Although these traditional models have offered valuable theoretical insights, they often overlook the complexity of real-world epidemics, such as structured quarantine processes, phased recovery, and heterogeneous vaccine responses. Hence, it is necessary to develop refined models that more accurately capture the dynamics of real epidemics.

In the past few years, several researchers have modified SEIR-type frameworks to incorporate critical public-health interventions. For instance, Mahadhika and Aldila[4] proposed a deterministic framework combining vaccination and quarantine mechanisms, but their approach only considered a single-stage isolation process. Rajput and Aggarwal[5] employed optimal-control and fractional-order techniques to enhance vaccination efficiency, yet their model did not include multiple quarantine compartments. Mishra[6] analyzed COVID-19 progression using a classical mathematical model but ignored multi-phase isolation and varying vaccine efficacies. Similarly, Lu and Borgonovo[7], Dagpunar and Wu[8], and Kumar and Santra[9] investigated stability, sensitivity, and vaccination effects; however, none of these studies simultaneously addressed structured multi-zone quarantine and imperfect vaccination within a single modeling framework. These gaps underline the need for a generalized model that realistically reflects epidemic interventions.

Recent research has also explored fractional-order epidemic models to capture memory effects and hereditary characteristics present in infection dynamics[10],[11],[12]. While fractional models can account for long-term dependencies and sub-diffusive behavior, they often involve greater analytical complexity and high computational demands, which limit closed-form stability analysis. In contrast, integer-order models provide better analytical tractability, allowing explicit computation of reproduction numbers and Lyapunov-based stability conditions. Therefore, the present study employs an integer-order approach that preserves both mathematical rigor and biological interpretability while maintaining computational efficiency.

To overcome the above limitations, we propose a generalized SEI$(\mathrm{Q}_1\mathrm{Q}_2\ldots\mathrm{Q}_{\mathrm{n}-4})$R model that integrates multiple quarantine zones, imperfect vaccination, and both natural and disease-induced mortality. During large-scale outbreaks such as COVID-19, infected individuals are commonly distributed across several healthcare facilities or isolation centers. The proposed model represents this reality by allowing transitions among multiple quarantine compartments, thereby offering a more realistic depiction of disease control interventions. This structured model better captures epidemic control mechanisms in densely populated or resource-limited settings.

The specific objectives of this study are to:

1. develop a generalized n-compartment SEI$(\mathrm{Q}_1\mathrm{Q}_2\ldots\mathrm{Q}_{\mathrm{n}-4})$R model incorporating vaccination and multi-level parallel quarantine structures;
2. derive the basic reproduction number and analyze the global stability of equilibrium points using Lyapunov techniques; and
3. conducted sensitivity and numerical simulation analyses to quantify and validate the theoretical outcomes, and to examine how vaccination efficacy, quarantine duration, and transmission parameters influence disease suppression. Sensitivity analysis highlights the parameters that exert the greatest impact on transmission dynamics, providing deeper insight into which factors most strongly govern the spread and control of infection. All parameter values were sourced from recent peer-reviewed literature to ensure biological realism during simulation experiments.

The findings of this work highlight the intricate interplay between multi-zone quarantine mechanisms and partial vaccination, illustrating how these interventions collectively influence epidemic progression. By integrating analytical rigor with public health relevance, the proposed integer-order framework offers a scalable and policy-oriented model adaptable to different epidemic complexities. Simulation validations for $n = 5$ and $n = 7$ further confirm the model's robustness and applicability for forecasting and guiding effective epidemic control strategies.

2 Methodology

2.1 Model formulation

We propose a deterministic compartmental framework represented as the SEI$(\mathrm{Q}_1\mathrm{Q}_2\ldots\mathrm{Q}_{\mathrm{n}-4})$R model, designed to capture the transmission pattern of an infectious disease incorporating both vaccination and multiple quarantine phases. At any instant t, the entire population $N(t)$ is classified into distinct and mutually exclusive groups: Susceptible $S(t)$, Exposed $E(t)$, Infectious

$I(t)$, Quarantined $Q_1, Q_2, \ldots Q_{n-4}$ and Recovered $R(t)$, where n- represents the total number of compartments in the system. The total population is defined as:

$$N(t) = S + E + I + \sum_{j=1}^{n-4} Q_j + R.$$

Individuals enter the susceptible compartment through recruitment at a constant rate A. From this class, they can either become infected through interaction with infectious individuals at rate $\beta(1-\phi v)$, successfully vaccinated at rate ϕv, or die naturally at rate d_1. The exposed individuals $E(t)$ carry the pathogen but are not yet infectious; they progress to the infectious group at a rate σ or die naturally at rate d_1. Infectious individuals $I(t)$ transition into several quarantine phases $Q_j(t)$ at rates γ_j (for $j = 1, 2, 3, \ldots, n-4$), and may experience disease-induced death at rate d_2 or natural mortality at rate d_1. Each quarantine class $Q_j(t)$ permits recovery at rate η_j, with both natural and disease-related deaths considered. Recovered individuals $R(t)$ increase via vaccination and recovery, and only natural mortality (rate d_1) is applied to this group. The corresponding schematic diagram is shown in Figure 1, and the parameter descriptions are listed in Table 1.

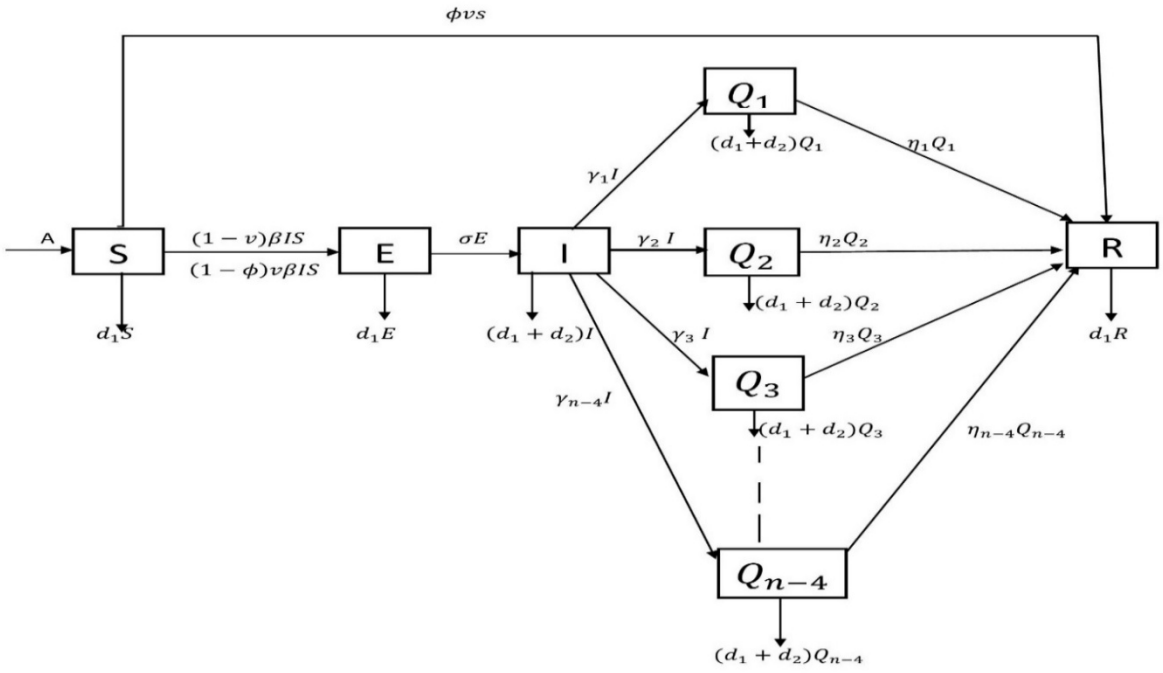

Fig 1. Schematic diagram of the n-compartment epidemiological model

The population is considered to mix uniformly, while vaccination offers partial and fixed efficacy $(v\epsilon(0,1))$. Only infectious and quarantined individuals are subject to disease induced death, whereas recovered individuals presumed to acquire lifelong immunity. The model can represent early outbreak control as well as endemic management depending on parameter choice.

Utilizing the specified parameters, assumed conditions, and the schematic representation of disease transmission, we establish a generalized n-compartmental model as:

$$\frac{dS}{dt} = A - \beta IS\,(1 - \phi v) - \phi vS - d_1 S$$

$$\frac{dE}{dt} = \beta IS\,(1 - \phi v) - \sigma E - d_1 E$$

$$\frac{dI}{dt} = \sigma E - \left(\sum_{j=1}^{n-4} \gamma_j + d_1 + d_2\right) I \tag{1}$$

$$\frac{dQ_j}{dt} = \gamma_j I - \left(\eta_j + d_1 + d_2\right) Q_j \text{ for } j = 1, 2, 3, \ldots, n-4$$

$$\frac{dR}{dt} = \phi v S + \sum_{j=1}^{n-4} \eta_j Q_j - d_1 R$$

where, $N' = S' + E' + I' + \sum_{j=1}^{n-4} Q_j' + R'$.

Table 1. Parameters Description

Symbols	Descriptions
β	Transmission rate between susceptible and infectious individuals
A	Recruitment rate into the susceptible population
σ	Rate at which exposed individuals become infectious
ϕ	Fraction of susceptible individuals vaccinated
v	Vaccine efficacy (fraction effectively immunized)
γ_j	Transition rate from infectious to the jth quarantine zone
η_j	Recovery rate from the jth quarantine zone
d_1	Natural mortality rate
d_2	Disease-induced death rate
$\Gamma = \sum_{j=1}^{n-4} \gamma_j$	Total transition rate to quarantine
$\eta = \sum_{j=1}^{n-4} \eta_j$	Total recovery rate from all quarantine zones

Assume the initial conditions $S(0)$, $E(0)$, $I(0)$, $Q_j(0)$, $R(0)$. Each differential equation in (1) contains nonnegative inflows and linear outflows proportional to the relevant state variables. Hence, all variables $(S(t),\ E(t),\ I(t),\ Q_j(t),\ R(t))$ remain nonnegative for every $t > 0$, ensuring biological feasibility. By summing **equations (1)**, we obtain

$$\frac{dN}{dt} < A - d_1 N,$$

which integrates to give

$$N(t) \leq \frac{A}{d_1} + \left(N(0) - \frac{A}{d_1}\right) e^{-d_1 t}.$$

Thus, $N(t)$ stays bounded above by $\frac{A}{d_1}$. Consequently, all model trajectories lie within the biologically meaningful region

$$\Omega = \left\{S,\ E,\ I,\ Q_j,\ R \in \mathbb{R}^n : S + E + I + \sum_{j=1}^{n-4} Q_j + R \leq \frac{A}{d_1}\right\}. \tag{2}$$

The region Ω is positively invariant, implying that the system is biologically consistent and all solutions remain finite and nonnegative. Also the right-hand sides of system (1) are continuously differentiable and locally Lipschitz in all variables, the Picard–Lindelöf theorem[13] guarantees both existence and uniqueness of solutions for any admissible initial condition within Ω. Therefore, the proposed system (1) is mathematically coherent and biologically realistic.

2.2 Existence of disease-free equilibrium (DFE)

To determine the DFE of the system (1), we assume no infection in the individuals. Hence, all infected compartments are set to zero: $E = I = Q_j = 0$. Substituting these values into the system (1), the remaining non-zero differential equations yield

$$S = \frac{A}{\phi v + d_1} \text{ and } R = \frac{\phi v A}{d_1 (\phi v + d_1)}.$$

Therefore, the DFE of the model (1) is given by

$$P_0 = \left(\frac{A}{\phi v + d_1}, 0, 0, 0, \ldots, \frac{\phi v A}{d_1 (\phi v + d_1)} \right). \tag{3}$$

This equilibrium corresponds to a disease-free population where all infected and quarantined compartments are zero, implying no infection circulation in the system.

2.3 Basic reproduction Number $(\mathcal{R}_0)$

The $\mathcal{R}_0$ is a fundamental metric in epidemiology that quantifies the average number of new infections caused by a single infectious individual in a population where everyone is susceptible. It provides insight into whether a disease has the capacity to spread or is likely to decline over time. Specifically, $\mathcal{R}_0 > 1$ indicates that the infection can propagate through the population, while $\mathcal{R}_0 < 1$ suggests that the disease will decline. For system (1), we evaluated $\mathcal{R}_0$ using the next-generation matrix methodology[14].

The infection subsystem of the model (1) includes the compartments

$$\mathcal{X} = [E, I, Q_1, Q_2, \ldots Q_{n-4}]^T.$$

Let $\mathcal{F}_j$ denotes the emergence rate of new infections in the j-th compartment and $\mathcal{V}_j$ the transfer dynamics of individuals across the infected categories, then

$$\mathcal{F}_j = \begin{bmatrix} 0 \\ \beta(1-\phi v) I S \\ 0 \\ \\ \\ \\ \end{bmatrix}, \quad \text{and} \quad \mathcal{V}_j = \begin{bmatrix} -(\sigma + d_1) E \\ \sigma E - (\gamma_j + d_1 + d_2) I \\ \gamma_1 - (\eta_1 + d_1 + d_2) Q_1 \\ \gamma_2 - (\eta_2 + d_1 + d_2) Q_2 \\ \\ 0 \end{bmatrix}.$$

With the help of Jacobian matrix, computing F and V by $F = \frac{\partial \mathcal{F}_j}{\partial \mathcal{X}}$ and $V = \frac{\partial \mathcal{V}_j}{\partial \mathcal{X}}$ as:

$$F = \begin{bmatrix} 0 & (1-\phi v)S & 0 & 0 & \cdots & 0 \\ 0 & 0 & 0 & 0 & \cdots & 0 \\ 0 & 0 & 0 & 0 & \cdots & 0 \\ 0 & 0 & 0 & 0 & \cdots & 0 \\ \vdots & \vdots & \vdots & \vdots & \vdots & \vdots \\ 0 & 0 & 0 & 0 & \cdots & 0 \end{bmatrix}, \quad \text{and}$$

$$V = \begin{bmatrix} -(\sigma + d_1) & 0 & 0 & 0 & \cdots & 0 \\ \sigma & -(\gamma_1 + \gamma_2 + \ldots + \gamma_{n-4} + d_1 + d_2) & 0 & 0 & \cdots & 0 \\ 0 & \gamma_1 & -(\eta_1 + d_1 + d_2) & 0 & \cdots & 0 \\ 0 & \gamma_2 & 0 & -(\eta_2 + d_1 + d_2) & \cdots & 0 \\ \vdots & \vdots & \vdots & \vdots & \vdots & \vdots \\ 0 & \gamma_{n-4} & 0 & 0 & \cdots & -(\eta_{n-4} + d_1 + d_2) \end{bmatrix}.$$

The matrix of next-generation type is formulated as FV^{-1}. Noting that matrix F contains only the (1,2) entry as nonzero and that V^{-1} is lower triangular, it follows that the product FV^{-1} has zero entries everywhere except at positions (1,1) and (1,2). The corresponding elements of V^{-1} are

$$V_{2,1}^{-1} = \frac{-\sigma}{(\sigma + d_1)(\sum_{j=1}^{n-4} \gamma_j + d_1 + d_2)} \text{ and } V_{2,2}^{-1} = \frac{-1}{\sum_{j=1}^{n-4} \gamma_j + d_1 + d_2}.$$

So, the matrix FV^{-1} is given by

$$FV^{-1} = \begin{bmatrix} \frac{-(1-\phi v)\beta\sigma S}{(\sigma+d_1)(\sum_{j=1}^{n-4}\gamma_j+d_1+d_2)} & \frac{-(1-\phi v)\beta S}{\sum_{j=1}^{n-4}\gamma_j+d_1+d_2} & 0 & 0 & \cdots & 0 \\ 0 & 0 & 0 & 0 & \cdots & 0 \\ 0 & 0 & 0 & 0 & \cdots & 0 \\ 0 & 0 & 0 & 0 & \cdots & 0 \\ \vdots & \vdots & \vdots & \vdots & \vdots & \vdots \\ 0 & 0 & 0 & 0 & \cdots & 0 \end{bmatrix}, \tag{4}$$

and $\mathcal{R}_0$ is computed as the largest absolute eigen-value of (4). We derive the following explicit formula

$$\mathcal{R}_0 = \frac{\beta(1-\phi v)\sigma A}{(\sigma+d_1)\left(\sum_{j=1}^{n-4}\gamma_j+d_1+d_2\right)(\phi v+d_1)}. \tag{5}$$

Biologically, $\mathcal{R}_0$represents the expected number of secondary infections generated by a single infectious individual in a fully susceptible population. Increasing vaccination coverage and vaccine efficacy (ϕv) or enhancing quarantine efficiency γ_j effectively reduces $\mathcal{R}_0$, thereby contributing to disease suppression.

2.4 Existence of endemic equilibrium (EE)

For $\mathcal{R}_0 < 1$, the system (1) does not support the presence of an EE. When $\mathcal{R}_0 > 1$, infection persists in the population, resulting in a positive steady state. Under this condition, we will establish the existence of a biologically feasible EE.

Let $P^*\ \left(S^*,\ E^*,\ I^*,\ Q_j^*,\ R^*\right) \in\ \Omega$ be the EE of system (1). Then it will satisfy the the steady-state equations of system (1) as:

$$A-\beta I^*\ S^*(1\ -\ \phi v)-\phi v\ S^*-d_1S^*=0 \tag{6}$$

$$\beta I^*S^*(1\ -\ \phi v)-\sigma E^*-d_1E^*=0 \tag{7}$$

$$\sigma E^*-\left(\sum_{j=1}^{n-4}\gamma_j+\ d_1+\ d_2\right)I^*=0 \tag{8}$$

$$\gamma_j I^*-\left(\eta_j+d_1+d_2\right)Q_j^*=0 \text{ for } j=1,\ 2,\ 3,\cdots n-4 \tag{9}$$

$$\phi v\ S^*+\ \sum_{j=1}^{n-4}\eta_j Q_j^*-d_1R^*=0 \tag{10}$$

On solving **equations (6) – (10)**, we obtain

$$S^*=\frac{(\sigma+d_1)C_1}{\beta(1-\phi v)\sigma};\ \text{where } c_1=\sum_{j=1}^{n-4}\gamma_j+d_1+d_2$$

$$E^*=\frac{C_1}{\sigma}\ I^*$$

$$I^*=\frac{1}{\beta(1-\phi v)}\left[\frac{A}{S^*}-(\phi v+d_1)\right] \tag{11}$$

$$Q_1^* = K_1^* I^*,\ Q_2 = K_2 I^*, \ldots,\ Q_{n-4} = K_{n-4} I^*;$$

$$\text{where } K_j = \frac{\gamma_j}{\eta_j + d_1 + d_2} \quad \forall \quad j = 1, 2, \ldots, n-4$$

$$R^* = \frac{1}{d_1}\left[\phi v S^* + \sum_{j=1}^{n-4} \eta_j K_j I^*\right].$$

It follows that $S^*,\ E^*,\ Q^*,\ R^* > 0$, and $I^* > 0$ if $\frac{A}{S^*} > \phi v + d_1$, which holds only when $\mathcal{R}_0 > 1$. Hence, a unique biologically feasible EE satisfying the coordinates given in **equation (11)** exists when $\mathcal{R}_0 > 1$, indicating the persistence of infection under inadequate control measures.

3 Results and discussion

3.1 Global asymptotic stability (GAS) of DFE

Here, we examine the global behavior of DFE of model (1). We introduce a threshold parameter defined by

$$\widetilde{\mathcal{R}}_0 = \frac{\beta(1-\phi v)A}{(\phi v + d_1)(\sum_{j=1}^{n-4} \gamma_j + d_1 + d\_2)}. \tag{12}$$

It is evident from the expressions (5) and (12) that $\mathcal{R}_0 < \widetilde{\mathcal{R}}_0$. So, $\widetilde{\mathcal{R}}_0 < 1$ implies $\mathcal{R}_0 < 1$ however, the converse implication is not guaranteed.

Theorem: 1. The DFE $P_0\left(\frac{A}{\phi v + d_1}, 0,\ 0,\ 0, \ldots,\ \frac{\phi v A}{d_1(\phi v + d_1)}\right)$ of the system (1) is GAS in the region (2), if $\mathcal{R}_0 < 1$.

Proof: We establish the global stability of P_0 by employing a suitable Lyapunov function

$$L_1 = E + I. \tag{13}$$

Differentiating (13) along system (1) obtained that

$$\dot{L}_1 = \dot{E} + \dot{I}$$

$$\leq\ I\left[\frac{\beta S(1-\phi v)}{\sum_{j=1}^{n-4} \gamma_j + d_1 + d_2} - 1\right]$$

$$\leq\ 0;\ \text{if } \widetilde{\mathcal{R}}_0 < 1.$$

Since, $\mathcal{R}_0 < \widetilde{\mathcal{R}}_0$, hence $\dot{L}_1 < 0$, if $\mathcal{R}_0 < 1$. Also, L_1 is radially unbounded. Thus, by LaSalle's principle[15], the DFE P_0 of the system (1) is GAS in the region (2), if $\mathcal{R}_0 < 1$. This implies that when $\mathcal{R}_0 < 1$, all infection-related variables $(E,\ I,\ Q_j)$ approach zero over time, leading to complete disease eradication. Biologically, this means that effective vaccination (ϕv) and efficient quarantine transitions (γ_j) are sufficient to suppress infection regardless of the initial population distribution. This result follows from the Lyapunov direct method and LaSalle's Invariance Principle, as applied in recent epidemiological modeling studies[15],[16],[17].

3.2 Global asymptotic stability (GAS) of EE

In the previous section **??**, we have obtained the explicit coordinate of EE. Now, we establish its dynamical behaviour.

Theorem: 2. The EE described in (11) of system (1) is GAS within the admissible region defined in (2) whenever $\mathcal{R}_0 > 1$.

Proof: The GAS of the EE is established using a Lyapunov techniques. To constructing the Lyapunov function at EE, we shift the origin to make our equilibrium point $(0,\ 0,\ 0, \ldots,\ 0)$. Introducing the transformation $S = s + S^*,\ E = e + E^*,\ I = i + I^*,\ Q_j = q_j + Q_j^* \forall\ j = 1,\ 2, \ldots, n-4$ and $R = r + R^*$ in system (1), the transformed system becomes

$$\frac{ds}{dt} = -\beta\left(is + I^* s + iS^*\right)(1-\phi v) - (\phi v + d_1)\, s$$

$$\frac{de}{dt} = \beta\left(is + I^* s + iS^*\right)(1-\phi v) - (\sigma + d_1)\, e$$

$$\frac{di}{dt} = \sigma e - \left(\sum_{j=1}^{n-4} \gamma_j + d_1 + d_2\right) i$$

$$\frac{dq_j}{dt} = \gamma_j i - \left(\eta_j + d_1 + d_2\right) q_j \text{ for all } j = 1,\ 2,\ 3,\ \cdots, n-4 \tag{14}$$

$$\frac{dr}{dt} = \phi v s + \sum_{j=1}^{n-4} \eta_j q_j - d_1 r$$

Let the Lyapunov function be,

$$L_2 = s + e + i\ + \textstyle\sum_{j=1}^{n-4} q_j + r \tag{15}$$

Differentiating (15) along the system (14), we obtained

$$\dot{L}_2 = \dot{s} + \dot{e} + \dot{i} + \sum_{j=1}^{n-4} \dot{q_j} + \dot{r}$$

$$= -d_1(s + e + i\ + q_1 + q_2 + \ldots + q_{n-4} + r).$$

So, we obtained $\dot{L}_2 < 0$, also L_2 is radially unbounded as $L_2 \to \infty$ if $(s,\ e,\ i,\ q_1, q_2, \ldots, q_{n-4}, r) \to \infty$. Hence by employing LaSalle's principle[15] the EE of system (1) is GAS.

This result confirms that when infection persists in the population and approaches a stable endemic state. Biologically, it represents a situation where vaccination and quarantine measures are insufficient to bring $\mathcal{R}_0$ below unity, leading to sustained transmission at equilibrium. The result is consistent with recent Lyapunov-based global stability studies in vaccination models[15], [16], [17].

3.3 Simulation Procedure

To validate the analytical results and examine the dynamic behaviour of the proposed $SEI(Q_1 Q_2 \ldots Q_{n-4})R$ epidemiological model and to asses the influence of quarantine heterogeneity, simulation were conducted using MATLAB (R2024a). The nonlinear system of ordinary differential equations was solved using Matlab's built-in Runge-Kutta (4,5) solver (ode45). For validation, results were cross-checked with a fourth-order Adams-Bashforth-Moulton (ABM4) predictor-corrector scheme, yielded a maximum relative error of $\varepsilon_{\max} = 1.55 \times 10^{-3}$, confirming numerical accuracy and stability with a uniform step size of h = 0.001. Both solvers produced nearly identical outcomes, confirming numerical consistency.

The total population was assumed to be $N(0) = 4000$, representing a moderately sized community outbreak. The initial compartmental distributions were set as S(0)=3600, $E(0) = 200$, $I(0) = 100$, $Q_1 = 40$, $Q_2 = 30$, $Q_3 = 20$ and $R(0) = 10$. These values represent an early epidemic phase in which approximately 90% of individuals are susceptible, while the remaining population is distributed among the exposed, infected, quarantined, and recovered compartments. In the absence of specific epidemiological data, these proportions were selected based on biologically plausible assumptions commonly adopted in early-stage epidemic modeling studies. The simulation was conducted over a 25-days period. Parameter values, as presented in Table 2, were selected based on validated literature to reflect realistic epidemic conditions. The transmission rate (β = 0.3) aligns with moderate infectious diseases such as COVID-19, as reported in Taghvei[10], while the progression rate from exposed to infected (σ = 0.2) corresponds to a typical 5-days incubation period supported by Ejima[18]. The recruitment rate (A = 0.27) ensures population balance, and the vaccination rate ($\phi = 0.3$) along with vaccine efficacy ($\upsilon = 0.5$) represent partial immunization coverage common in public health rollouts, supported by data from De Leon[19] and Zhao[20] respectively. The natural death rate ($d_1 = 0.00004$) corresponds to an average life expectancy of about 70 years, and the disease-induced death rate ($d_2 = 0.02$) reflects mortality rates from acute respiratory infections. These parameter choices ensure that the model realistically captures the dynamics of infectious disease spread under quarantine interventions.

Table 2. Parameters value for EE

Symbol	Description	Value	Source
β	Transmission rate	0.3	Taghvaei et al., (2020)[10]
σ	Incubation rate	0.2	Ejima et al., (2021)[18]
A	Recruitment rate	0.27	Assumed based on demographic balance
ϕ	Vaccination rate	0.3	De Leon et al., 2021[19]
υ	Vaccine efficacy	0.5	Zhao, X., (2022)[20]
d_1	Natural mortality rate	0.00004	Assumed based on life expectancy (70 years)
d_2	Disease induced death	0.02	Assumed-based for acute respiratory infections
γ_1, γ_2, γ_3	Quarantine transition rates	0.18, 0.14, 0.08	Assumed for moderate quarantine policy
η_1, η_2, η_3	Recovery rates	0.40, 0.30, 0.20	Assumed for average recovery time (3–14 days)

In the baseline scenario, all quarantine zones were aggregated into a single equivalent compartment $SEIQ_1R$. The total quarantine transition rate $\Gamma = \sum \gamma_j = 0.4$ and the recovery rate from quarantine $(\eta = \sum \eta_j = 0.3)$ were chosen to capture the effects of timely isolation and average recovery durations of 5–21 days. The trajectories obtained using the ode45 solver are presented in Figure 2. The susceptible population $S(t)$ declines rapidly due to transmission, while the exposed $E(t)$ and infected $I(t)$ compartments initially increase and subsequently decrease as recovery becomes dominant. The recovered population $R(t)$ rises steadily, reflecting effective containment and gradual progression toward stability under uniform isolation.

To capture the heterogeneity in quarantine implementation, the model incorporates three parallel quarantine compartments Q_1, Q_2 and Q_3- representing mild, moderate, and critical isolation respectively, capturing heterogeneity in medical supervision and resource intensity. The total quarantine transition rate was fixed at $\Gamma = 0.4$ and distributed among the zones as $\gamma_1 = 0.18$, $\gamma_2 = 0.14$, and $\gamma_3 = 0.08$, reflecting the relative accessibility and utilization of these isolation categories. Similarly, distinct recovery rates were assigned to each quarantine level, with $\eta_1 = 0.4$, $\eta_2 = 0.30$, and $\eta_3 = 0.2$, representing faster recovery for mild cases and prolonged recovery durations for severe infections. The effective recovery rate for the parallel quarantine structure was maintained at $\eta = 0.3$, to ensure equivalence with the baseline single-zone scenario. While the overall quarantine intensity remained constant, the parallel configuration allowed infected individuals to be distributed across multiple isolation environments, reducing overburdening of any single facility. The corresponding simulation outcomes, illustrated in Figure 3, demonstrate smoother infection peaks and faster convergence toward equilibrium compared to the single-zone model. The presence of multiple quarantine zones enables distributed isolation efforts, reducing crowding within a single zone and thereby lowering the overall infection pressure on the susceptible population. This parallel quarantine configuration enhances containment efficiency and shortens the overall epidemic duration, emphasizing the importance of heterogeneous quarantine implementation in disease control.

All state variables remained positive throughout the integration process, thereby preserving biological feasibility and confirming computational reliability. For the given parameter set $(\upsilon = 0.5)$, the basic reproduction number was determined to be $\mathcal{R}_0 > 1$, indicating endemic persistence. When the vaccine efficacy was increased to $\upsilon = 0.6$, $\mathcal{R}_0$dropped below unity, confirming successful disease suppression. Simulations with extended compartmental structures ($n = 5$ and $n = 7$) exhibited consistent dynamical patterns, validating the scalability and robustness of the proposed model.

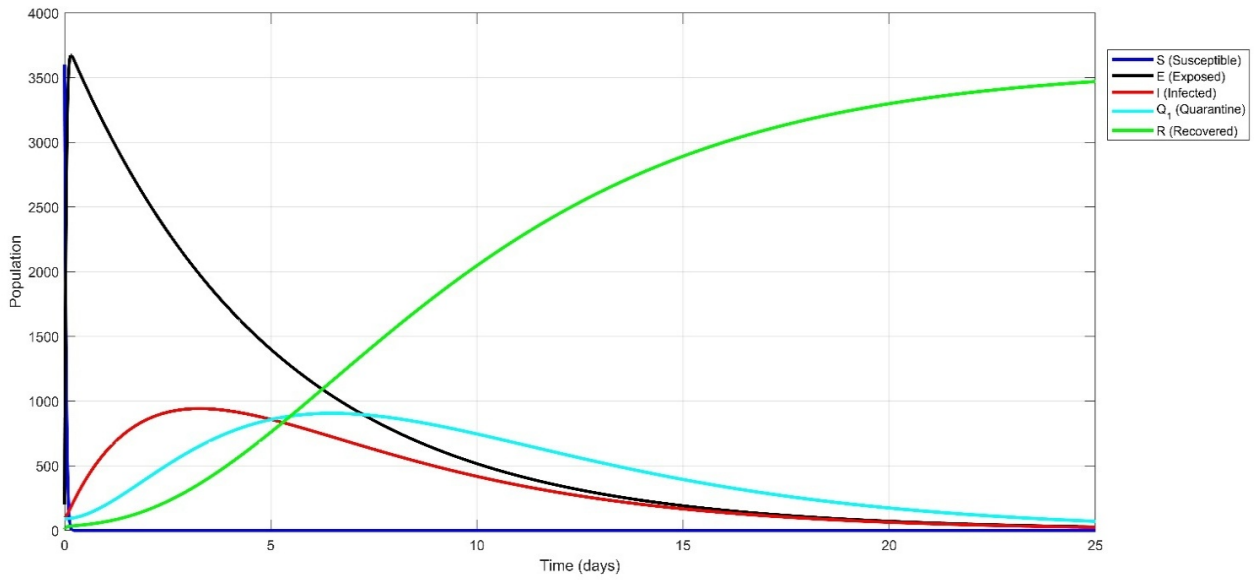

Fig 2. MATLAB (R2024a) simulation of the aggregated $SEIQ_1R$ model showing the temporal evolution of epidemic compartments

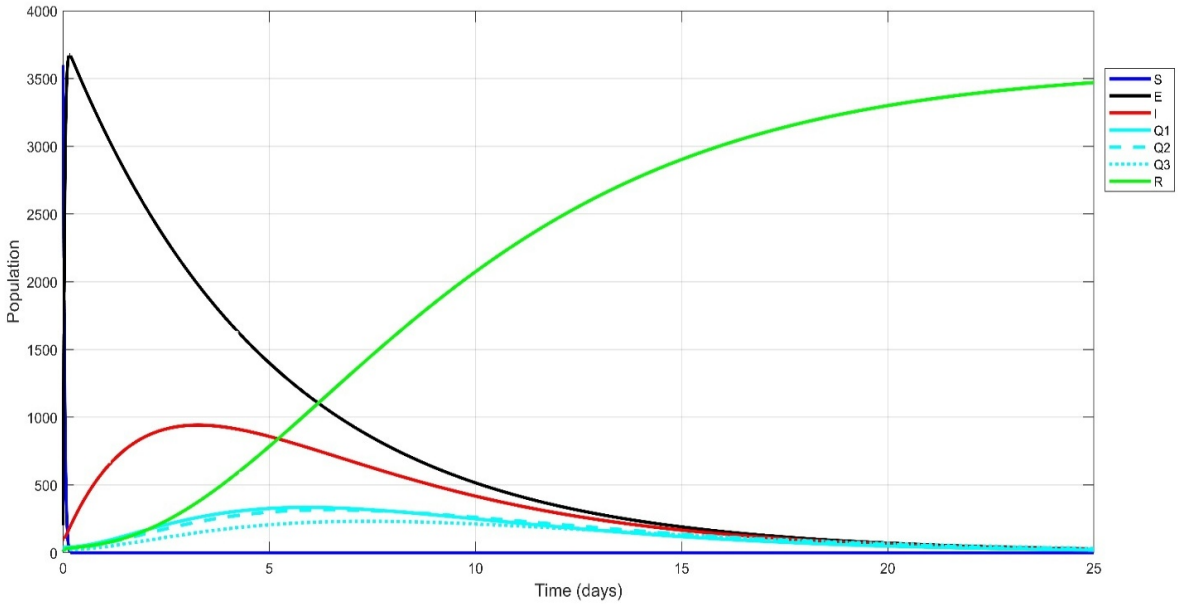

Fig 3. Simulation of the $SEI(Q_1Q_2Q_3)R$ model demonstrating enhanced stability and smoother infection peaks through phased quarantine

3.4 Sensitivity analysis

A sensitivity analysis of the $\mathcal{R}_0$, illustrated by **equation (5)**, was conducted to assess the impact of various epidemiological factors on disease transmission. This method allows us to pinpoint which parameters most significantly affect on $\mathcal{R}_0$, thereby indicating their role in shaping the outbreak of disease potential. Following the method described in Samui[21], the normalized sensitivity index of $\mathcal{R}_0$ for parameter x takes the form:

$$S_x^{R_0} = \frac{\partial R_0}{\partial x} \frac{x}{R_0} \tag{16}$$

Table 3. Sensitivity Indices

Parameters	Baseline Value	Sensitivity Indices
β	0.3	1.000
σ	0.2	0.0002
A	0.27	1.000
ϕ	0.3	-1.1762
υ	0.2	-1.1762
d_1	0.00004	-0.0060
d_2	0.02	-0.0476
$\Gamma = \sum \gamma_j$	0.4	-0.9523

By utilizing the parameter values specified in Table 2, estimated the indices of sensitivity for all variables concerned with **equation (5)**, results are listed in Table 3. These indices provide insight into how changes in each parameter may affect the reproduction number and, in turn, the overall dynamics of disease transmission.

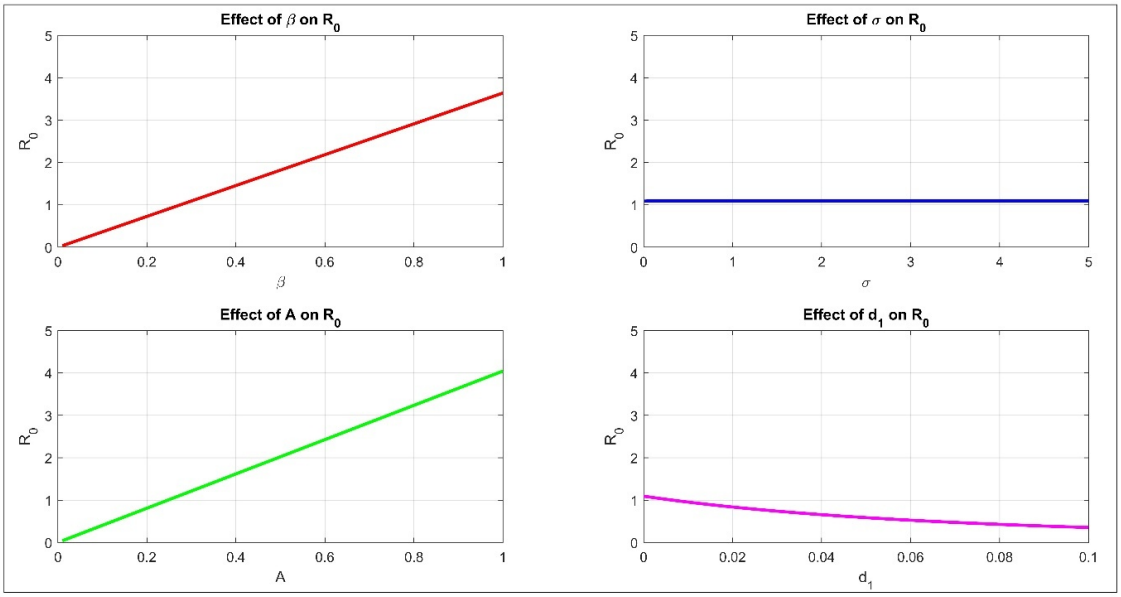

Fig 4. Sensitivity analysis showing the effect of key parameters β, σ, A and d_1 on R_0

From Table 3, the sensitivity indices associated with parameters such as ϕ, υ, d_1, d_2 and Γ are found to be negative, implying that enhancing these values would result in a reduction of the R_0. In contrast, parameters including β, A and σ exhibit positive sensitivity indices, which means that any increase in these factors would cause R_0 to rise. If we increase 10% in β, there will 10% increase in the R_0 and decrease 10% in ϕ, υ and Γ there will 11.762%, 11.762% and 9.523% decrease in the R_0 respectively. Figure 4 and Figure 5 are MATLAB (R2024a) - generated plots demonstrating the impact of $\mathcal{R}_0$ on individual parameters, produced by altering one parameter at a time while keeping all others constant at baseline levels.

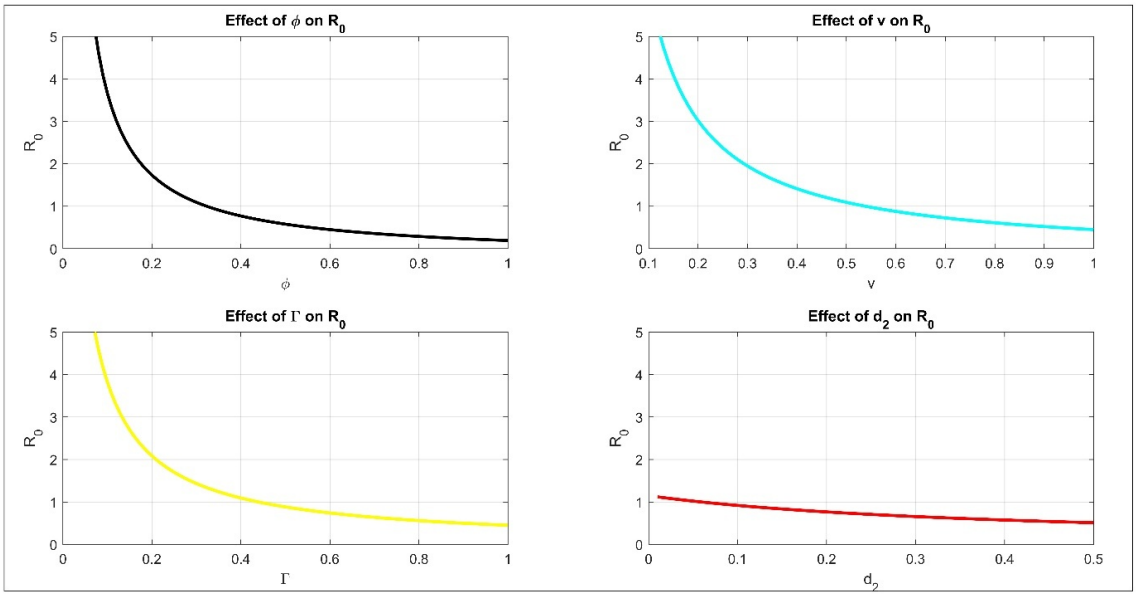

Fig 5. Sensitivity analysis showing the effect of key parameters ϕ, v, Γ and d_2 on R_0

4 Conclusions

This study developed a generalized nnn-compartmental SEI($Q_1Q_2\ldots Q_{n-4}$)R epidemiological model that incorporates multiple quarantine phases and vaccination to more effectively capture the influence of isolation, recovery, and immunization interventions during infectious disease outbreaks. The model integrates key epidemiological mechanisms such as vaccination coverage, quarantine transition, and demographic dynamics. Lyapunov-based analysis established the global asymptotic stability of the disease-free equilibrium when and the endemic equilibrium when . Numerical simulations for n=5 and n=7, supported by MATLAB (R2024a), validated the theoretical results, demonstrating consistency across different solver schemes and confirming model scalability. Sensitivity analysis further identified transmission rate, vaccination coverage, vaccine efficacy, and recovery rate as critical determinants of R0R_0R0, underscoring their importance in epidemic control.

Overall, the proposed integer-order SEI($Q_1Q_2\ldots Q_{n-4}$)R framework provides an analytically rigorous and biologically realistic foundation for assessing the combined impact of quarantine and vaccination strategies. The model's adaptable structure makes it suitable for diverse outbreak scenarios, contributing to evidence-based epidemic forecasting and public health policy design.

Despite its strengths, the model assumes homogeneous mixing and permanent immunity, which may not fully capture real-world complexity. Future extensions may include stochastic effects, age-structured or spatially heterogeneous populations, and multi-dose vaccination schemes to enhance predictive realism and applicability.

References

1) Cooper I, Mondal A, Antonopoulos CG. A SIR model assumption for the spread of COVID-19 in different communities. *Chaos, Solitons & Fractals*. 2020;139:110057. 10.1016/j.chaos.2020.110057.
2) Chakraborty T, Ghosh I. Real-time forecasts and risk assessment of novel coronavirus (COVID-19) cases: A data-driven analysis. *Chaos, Solitons & Fractals*. 2020;135:109850. 10.1016/j.chaos.2020.109850.
3) Ivorra B, Ferrández MR, Vela-Pérez M, Ramos AM. Mathematical modeling of the spread of the coronavirus disease 2019 (COVID-19) taking into account the undetected infections. The case of China. *Communications in Nonlinear Science and Numerical Simulation*. 2020;88:105303. 10.1016/j.cnsns.2020.105303.
4) Mahadhika CK, Aldila D. A deterministic transmission model for analytics-driven optimization of COVID-19 post-pandemic vaccination and quarantine strategies. *Mathematical Biosciences and Engineering*. 2024;21(4):4956–4988. 10.3934/mbe.2024219.
5) Rajput A, Sajid M, Tanvi, Shekhar C, Aggarwal R. Optimal control strategies on COVID-19 infection to bolster the efficacy of vaccination in India. *Scientific Reports*. 2021;11(1):20124. 10.1038/s41598-021-99088-0.
6) Mishra BK, Keshri AK, Saini DK, Ayesha S, Mishra BK, Rao YS. Mathematical model, forecast and analysis on the spread of COVID-19. *Chaos, Solitons & Fractals*. 2021;147:110995. 10.1016/j.chaos.2021.110995.

7) Lu X, Borgonovo E. Global sensitivity analysis in epidemiological modeling. *European Journal of Operational Research*. 2023;304(1):9–24. 10.1016/j.ejor.2021.11.018.
8) Dagpunar J, Wu C. Sensitivity of endemic behaviour of COVID-19 under a multi-dose vaccination regime, to various biological parameters and control variables. *Royal Society Open Science*. 2023;10:221277. 10.1098/rsos.221277.
9) Kumar RP, Santra PK, Mahapatra GS. Global stability and analysing the sensitivity of parameters of a multiple-susceptible population model of SARS-CoV-2 emphasising vaccination drive. *Mathematics and Computers in Simulation*. 2023;203:741–766. 10.1016/j.matcom.2022.07.012.
10) Taghvaei A, Georgiou TT, Norton L, Tannenbaum A. Fractional SIR epidemiological models. *Scientific Reports*. 2020;10:20882. 10.1038/s41598-020-77849-7.
11) Rajagopal K, Hasanzadeh N, Parastesh F, et al. A fractional-order model for the novel coronavirus (COVID-19) outbreak. *Nonlinear Dynamics*. 2020;101:711–718. 10.1007/s11071-020-05757-6.
12) Alcántara-López F, Fuentes C, Chávez C, Brambila-Paz F, Quevedo A. Fractional growth model applied to COVID-19 data. *Mathematics*. 2021;9(16):1915. 10.3390/math9161915.
13) Ottaviano S, Sensi M, Sottile S. Global stability of SAIRS epidemic models. *Nonlinear Analysis: Real World Applications*. 2022;65:103501. 10.1016/j.nonrwa.2021.103501.
14) Appiah BK, Fosu GO. Next-generation matrix application in COVID-19 basic reproduction number calculation for compartmental models. *Open Journal of Mathematical Sciences*. 2023;11:456. 10.30538/oms2020.0117.
15) Kumar PR, Basu S, Ghosh D, Santra PK, Mahapatra GS. Dynamical analysis of novel COVID-19 epidemic model with non-monotonic incidence function. *Journal of Public Affairs*. 2022;22:e2754. 10.1002/pa.2754.
16) Naji RK, Hussain HA. Global stability of SEIR epidemic models with vaccination and treatment. *Alexandria Engineering Journal*. 2021;60(4):4021–4032. 10.1016/j.aej.2021.02.065.
17) Vargas-De-León C. Stability analysis in epidemiological models using Lyapunov functions. *Applied Mathematical Modelling*. 2022;103:385–398. 10.1016/j.apm.2021.10.021.
18) Ejima K, Kim KS, Ludema C, Bento AI, Galvani AP. Estimation of the incubation period of COVID-19 using viral load data. *Epidemics*. 2021;35:100453. 10.1016/j.epidem.2021.100454.
19) De-Leon H, Pederiva F. Statistical mechanics study of the introduction of a vaccine against COVID-19 disease. *Physical Review E*. 2020;104(1):014132. 10.1103/PhysRevE.104.014132.
20) Zhao X, Tatapudi H, Corey G, Gopalappa C. Threshold analyses on combinations of testing, population size, and vaccine coverage for COVID-19 control in a university setting. *PLoS One*. 2021;16(8):e0255864. 10.1371/journal.pone.0255864.
21) Samui P, Mondal J, Khajanchi S. A mathematical model for COVID-19 transmission dynamics with a case study of India. *Chaos, Solitons & Fractals*. 2020;140:110173. 10.1016/j.chaos.2020.110173.